Investigation of pulse shape characteristics on the laser ablation dynamics of TiN coatings in ns regime

Ali Gökhan Demir[1]*, Krste Pangovski[2], William O'Neill[2], Barbara Previtali[1]

[1]Department of Mechanical Engineering, Politecnico di Milano, Via La Masa 1, 20156 Milan, Italy

[2]Institute for Manufacturing, University of Cambridge, 17 Charles Babbage Road, Cambridge, CB3 0FS, United Kingdom

*Corresponding author; aligokhan.demir@polimi.it

Investigation of pulse shape characteristics on the laser ablation dynamics of TiN coatings in ns regime

Ali Gökhan Demir[1]*, Krste Pangovski[2], William O'Neill[2], Barbara Previtali[1]

[1]Department of Mechanical Engineering, Politecnico di Milano, Via La Masa 1, 20156 Milan, Italy

[2]Institute for Manufacturing, University of Cambridge, 17 Charles Babbage Road, Cambridge, CB3 0FS, United Kingdom

*Corresponding author; aligokhan.demir@polimi.it

Abstract

In this work, the ablation dynamics of TiN coating with a ns-pulsed fibre laser in a wide range of pulse durations were studied. Critical time instances within the pulse duration were assessed by reflected pulse analysis. Digital holography was employed to investigate the shock wave expansion dynamics within and beyond the pulse duration. The results depict that the absorption behaviour changes as a function of the pulse rise time. Moreover, planar expansion of the shock wave is observed, which is generally linked to higher machining quality and absence of excessive plasma. The results of the study are interpreted to depict the required characteristics of optimized pulse shapes in ns-region for improved micromachining performance.

Keywords: Laser ablation, digital holography, plasma dynamics, pulse shape design

1. Introduction

Laser ablation is used for various purposes: for material analysis in analytical chemistry [1], for material synthesis [2] or deposition [3,4], as a tool in surgery [5], and widely for material processing in micro applications [6]. Different processes based on ablation, namely marking, drilling and engraving, are commonly applied with high brilliance pulsed fibre laser sources operating with ns pulse duration. The ns-pulsed lasers provide better machining quality compared to ms and μs pulsed sources, since heat diffusion is limited to shorter time extent. The larger diffusion of ns-pulsed fibre lasers is a consequence of different factors, mainly regarding machining quality, feasibility of operation and costs. Based on solid state active media, fibre laser

2

sources allow lower production costs and more stable operation. Furthermore today's fibre lasers employed in the industry are characterized by pulse energies up to 1-2 mJ with kHz level repetition rates and high quality beams that generate small spots. Another factor that adds higher flexibility in operation and consequently receives further attention from both industrial and research communities is the control over the pulse duration and shape. The control over the pulse duration and shape enables a larger band of tunability in terms of a compromise between machining quality and high productivity. Within the time scale of tens of ns, the material absorbs the deposited energy, which is transferred to the lattice that can generate both melt and vapour phases. Depending on the material physical properties and the pulse profile, it is possible to deposit energy in a controlled manner in time, enabling different material mechanisms to occur such as melt expulsion, explosive boiling, direct vaporization or vaporization from melt phase, which can be opportunely used to remove material with higher efficiency or better quality [7]. Industrially, pulse duration and profile selection is applied to match the requirements of specific micromachining process. There is relatively little information on the physical reality that determines the processing conditions. Previous works have been focused on ablation physics of low intensity beams with high energy content, which are not industrially employed for machining purposes. Most of the analysis lack the information regarding the pulse duration and shape. On the other hand, ns-pulsed laser ablation of TiN coatings was studied in single and multiple pulses previously [8]. The effects of pulse peak and tail have been shown on the ablation quality and efficiency empirically. In particular on TiN, the pulse peak has been found to initiate ablation and the tail to increase its extent. The added energy in the tail resulted only in the saturation of the ablation region. The experimental results depicted for better machining quality, fast ascending pulses that are no longer than 65 ns in duration were favourable. The analysis on large experimental conditions are useful to practically identify the optimal machining conditions. However, they do not provide clear information on the phenomenon occurring within the process that determine the machining quality. Indeed better comprehension of the mechanisms is required for further improvement of the machining quality with the ns-pulsed lasers, by monitoring the phenomenon within and beyond the pulse duration. Use of monitoring strategies are fundamental for identifying critical time instances in the laser-matter interaction. Such information can be useful both for the development of future generation laser sources as well as for the optimization of existing processes.

3

In the majority of published work dealing with laser ablation, empirical approaches have been employed to identify the best machining conditions. Various works modelling ablation of different materials using analytical and numerical methods have also been proposed in the literature [5,9-11]. On the other hand, several techniques for monitoring ablation dynamics can be employed for a direct observation of the ablation plume and shock wave. The monitoring methods are mainly based on optical approaches such as probe beam deflection [12,13], shadowography [14-19], schlieren photography [20], interferometry [21,22] and digital holography [23-26]. The previous works in the literature have provided a better understanding of the ablation phenomenon in general. A further step should be taken to also identify the critical pulse components to make recommendations for pulse shape design. As shown in this work, some of these methods are highly useful for this purpose to construct a methodology for pulse shape study and design recommendation purposes.

This paper describes a method to investigate the pulse shape characteristics to identify critical points for pulse shape design. Two different techniques were used namely, reflected pulse analysis and digital holography, to identify the ablation characteristics with ns pulses of different durations on TiN ceramic coating, a highly interesting material for mechanical [27], electronical [28], and biomedical [29] applications. For a better comprehension of the pulse characteristics, single pulse ablation conditions were tested, since it generates the simplest block for more complex micromachining processes based on multiple pulses. Reflected pulse analysis is based on the comparison of the pulse shape reflected from the machined material with its non-altered shape. This technique enables high temporal resolution in time and identifies characteristic points within the pulse duration itself. On the other hand digital holography was used to observe the shock wave expansion in single pulse ablation, which allows extracting information on the spatial behaviour linked to the heat source and released energy. The results are used to identify the critical temporal and spatial pulse characteristics for improved laser micromachining quality, as the recommendations for pulse shape are given in the end.

2. Experimental

2.1. Processing and monitoring systems

The material used for the experimentation was TiN coating deposited by physical vapour deposition (PVD) on AISI M2 tool steel. The coating thickness was measured as 4.0 ± 0.2 μm.

The experimental setup consisted of the following 3 principal components:

- Processing laser

- Reflected pulse analysis section

- Digital holography system

The laser source used for the processing of the TiN coating was an active fibre laser with master oscillator pulse amplifier (MOPA) architecture (G4 from SPI, Southampton, UK). The laser source emitted at 1064 nm wavelength (λ). The pulse shape selection of the processing laser allowed using pulse durations (τ) between 12-200 ns with pulse energy (E) up to 800 µJ. The laser was focused with a 75 mm focal lens (see Table I for the main characteristics). For the experiments 4 pulse shapes were selected with 30 ns, 40 ns, 100 ns, and 200 ns durations (see Figure 1). The pulse energy conditions were matched to obtain same pulse peak power at 3.4 kW generating 1.3 GW/cm^2 peak irradiance for all pulse durations. In these conditions pulses with 30 ns and 40 ns durations were characterized by a Gaussian-like shape with symmetry around the pulse peak power instance. The longer pulses with 100 ns and 200 ns durations exhibited fast ascending peaks and slow decaying tails. Resultantly the pulse energies were 47 µJ, 69 µJ, 172 µJ, and 300 µJ for 30 ns, 40 ns, 100 ns, and 200 ns durations respectively.
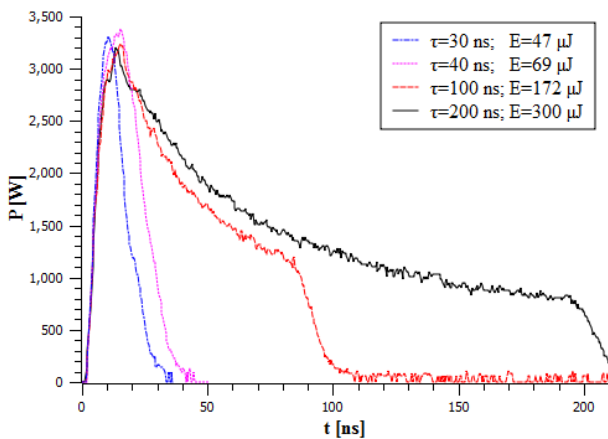

Figure 1. Pulse profiles belonging to different pulse durations employed in the experiments.

The second component of the experimental setup, the reflected pulse analysis section, consisted of a beam splitter and two photo detectors (PD1 and PD2) to observe the shape of the incoming and reflected beams as depicted in Figure 2. The used beam splitter (DMLP900 from Thorlabs, Newton, New Jersey, USA) allowed

96.3% of the light intensity of the laser wavelength to be transmitted, whereas the 3.52% of the intensity was reflected and captured by photo detector 1 (PD1) (DET10A/M from Thorlabs). The reflected laser beam from the work piece was bounced back from the same beam splitter and captured by the photo detector 2 (PD2). The photo detector 2 (PD2) was coupled to a line filter at the laser wavelength (FL1064-3 from Thorlabs) to avoid the process emission in visible and invisible spectrum to be captured as well (central wavelength 1064 nm, FWHM = 3 nm). The reflected pulse shapes were used to identify the characteristic time instances, where significant changes in the reflectance changed. For this reason they were not normalized, but the pulse shapes were compared with the present scale in electrical voltage.

Table I. Main characteristics of the laser sources used for material processing and for imaging in the digital holography system.

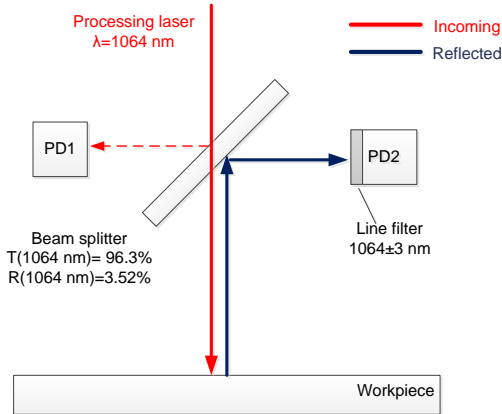|	Processing	Imaging
Brand and model	SPI G4	TEEM PNG-M04005
Emission wavelength, λ	1064 nm	532 nm
Pulse duration, τ	30-220 ns	400 ps
Average output power, P_{avg}	20 W	0.045 W
Pulse repetition rate, PRR	1-500 kHz	0.01-0.5 kHz
Maximum pulse energy, E_{max}	800 µJ	45 µJ
Beam quality factor, M^2	≤1.3	≤1.3
Collimated beam diameter, d_c	5.5 mm	1.2 mm

Figure 2. The elements of the reflected pulse analysis system to observe the differences in the shape of the incoming and reflected pulses.

The third component of the experimental setup was the digital holography system, with Fresnel off-axis holography geometry (see Figure 3). The imaging laser was a passively Q-switched microchip laser with central emission wavelength at 532 nm, and emitting pulses with 400 ps duration (PNG-M02010 from Teem Photonics, Grenoble, France). See Table I for the main characteristics of the imaging laser. The measured coherence length of the laser was approximately 10 mm. The output beam was spatially filtered to produce a clean collimated Gaussian beam. The beam was then split using a polarization insensitive 50:50 beam splitter (BS1). The reference beam was launched into a single mode fiber and delivered directly to the CCD detector. The probe pulse was free-space delivered. The beam passed through a beam expander to allow full illumination of the induced phase object, which is imaged onto a diffuser (D). The diffuser was imaged directly onto the CCD of the camera using a 4f imaging system (IS). A bandpass filter ($\lambda = 532$ nm, FWHM = 1 nm) was used to suppress plasma luminescence. The probe and reference wavefronts were allowed to interfere directly on the CCD which was placed in the focal plane of the imaging system. For this purpose a fast-shutter CCD camera with 6.7 µm x 6.7 µm pixel size, 12 bit dynamic range and a shutter speed of 100 ns was used (Sensicam from PCO, Kelheim, Germany). In this configuration the temporal resolution of the system is determined by the pulse duration of the imaging laser (400 ps). The field of view of the obtained images was 1.8 x 1.8 mm². Different time instances within the ablation process were captured by varying the time delay between the processing and the imaging pulses via a delay generator (DG353 from Stanford Research Systems, Sunnyvale, CA, USA). For each time instance a different laser pulse ablating a separate point on the material surface was used. The images belonging to undisturbed air were recorded as the reference image each time prior to the

7

exposure of the material to the processing laser pulse. Reference images were digitally compared with the images recorded after the processing pulse to obtain the wrapped phase maps, which were then unwrapped digitally to obtain continuous phase maps.
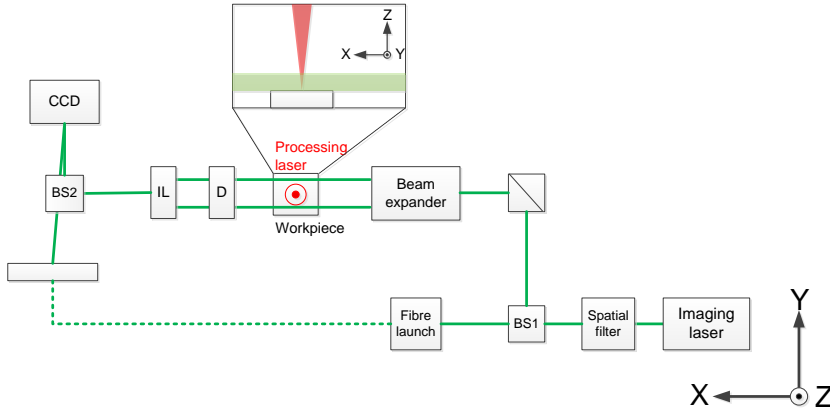

Figure 3. Digital holography system used to observe shock wave propagation.

2.2. Experimental procedure

In the first phase, reflected pulse analysis was carried out for the chosen pulse durations. Incoming and reflected pulses were recorded during single pulse ablation on TiN. Five replications were made for each case. The rise time of the incoming pulse was measured as the duration to reach the peak pulse intensity. The reflected pulses showed a saddle point in the pulse peak, which was defined as the peak absorption point. The duration to reach the peak absorption was also measured and compared to the rise times of the pulses.

In the second phase digital holography images of the shock wave induced by the single laser pulse on TiN were acquired. The shock wave propagation was observed in different time instances with respect to the arrival of a single pulse. Each time a new pulse was sent over different positions of the TiN specimen to acquire different time instances to generate a time lapse sequence of the shock wave expansion. The phase maps were used to measure the wave front radius in horizontal (r_{hor}) and vertical (r_{ver}) axes, as seen in Figure 4. The holographic images were acquired until the shock wave front was within the field of view, thus up to 5 µs of delay.
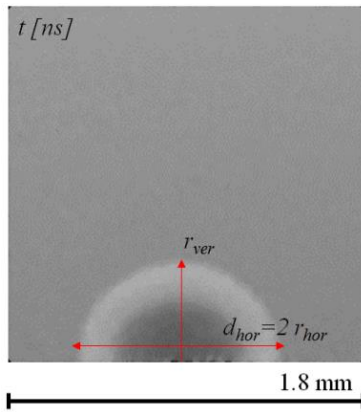
8

Figure 4. Definition of the shock wave extent in vertical and horizontal axes.

3. Results and discussion

3.1. Reflected pulse analysis

Figure 5 shows the reflected pulse shapes of the different pulse durations. It can be observed that for pulse durations between 40 ns and 200 ns the peak absorption is present as depicted by the arrows. On the other hand the peak absorption was not present with the 30 ns pulses. The pulse shape was consistent and remained Gaussian with the 30 ns pulses, whereas the longer ones showed steeper decay in the tail compared to the incoming pulse shape. Constant reflectivity would result in the attenuation of the pulse intensity, maintaining the shape. This fact points out that the absorption characteristics vary within the pulse itself. After the occurrence of the peak absorption, the energy within the tail is expected to couple better to the material, thus changing the shape of the reflected pulse in the tail. Similar observations were made by Xu et al [30]. The authors showed that the reflected pulse shape remains similar to the incoming 30 ns pulses, when the irradiance level is below laser supported detonation (LSD) threshold. Instead, when the irradiance level exceeds the threshold, similar peak absorption is observed. They associated the drop in the reflected pulse shape to the initiation of the LSD. LSD occurs when the precursor shock is strong enough to heat the surrounding gas, leading it to absorb the laser energy [31]. Resultantly, the LSD wave propagates towards the laser pulse and causes loss of symmetry in the expanding shock wave. Higher laser intensities can also cause breakdown in air [17,23]. Both of these conditions generate loss of energy transfer to the machined material and scatter the laser light causing degraded machining quality. In this work, none of the tested conditions generated LSD or air breakdown. However, plasma generation in the early phase of the pulse duration or melt generation may

be the source of increased absorption. For 100 and 200 ns pulses, the reflected pulse shape oscillating behaviour is present throughout the tail. This fact is attributed to the presence of melt varying the absorption until the end of the pulse duration. The 40 ns pulse duration shows the traces of oscillation phenomenon in the last 10 ns. The oscillating behaviour is absent in the case of 30 ns, since the reflected pulse is only an attenuated form the of the incoming pulse.
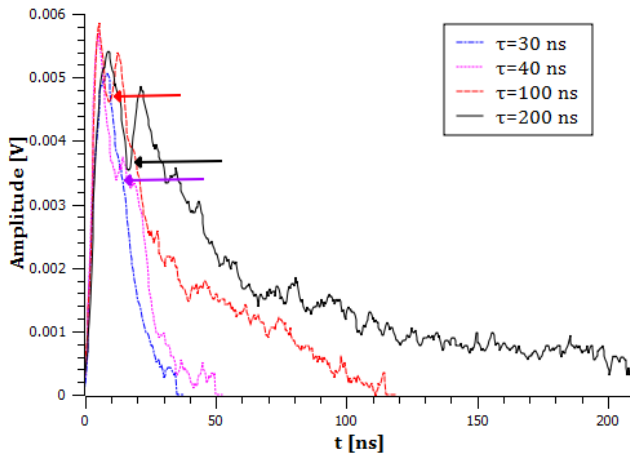

Figure 5. Shapes of the reflected pulses. The pulses durations between 40-200 ns show sudden drops after the peak, which are indicated by arrows.

In Figure 6 the rise times of the different pulse durations are compared to the time instance of peak absorption occurrence. The analysis of variance (ANOVA) confirmed that the rise times of 40 ns, 100 ns and 200 ns are statistically the same with 5% significance level (average t_{rise}=16 ns; group B). Peak absorption occurs at a time instance shorter than the rise times (average $t_{peak\ abs}$=14 ns; group C), whereas the rise time of the 30 ns pulses is shorter than the previous two (average $t_{rise,}$=10 ns; group A). The results imply that the faster rising 30 ns pulses interact with the material with constant absorption, avoiding plasma coupling or melt generation. The ablated zones were observed and found to be free of melt for 30 ns and 40 ns pulses. On the other hand melt formation around the edges of the ablated area was visible for 100 ns and 200 ns pulses (see Figure 7). This fact is inline with the observed oscillation behaviour in the reflected pulse shapes. It is worthwhile to notice that the machining quality is determined by relatively small differences such as 6 ns of difference in the rise time. Moreover, 40 ns appears to be near the limit to maintain quality as it shows the initial signs of melt generation.
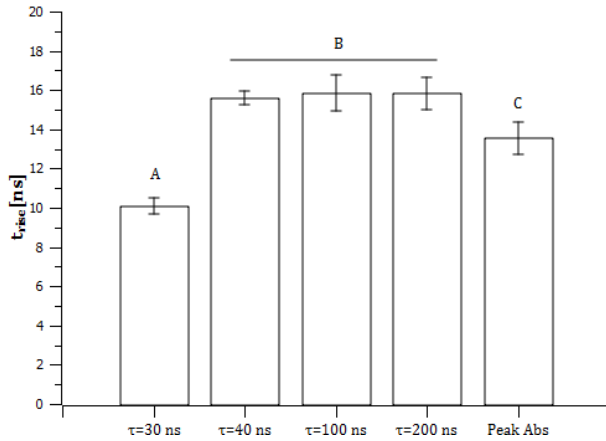
Figure 6. Comparison of rise times of different pulse durations and the peak absorption observed in 40 ns, 100 ns and 200 ns pulses. A, B and C groups are statistically different.
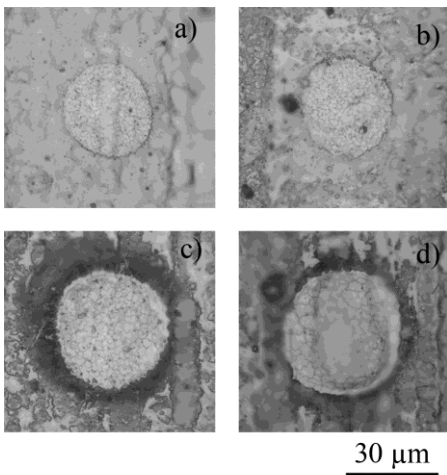

Figure 7. Optical microscope images of the ablated areas using single pulses of a) 30 ns, b)40 ns, c) 100 ns, and d) 200 ns duration.

3.2. Shock wave expansion

The holographic images showed semi-spherical shock wave geometry for all the pulse durations. Figure 8 reports the shock wave expansion in intermediate stages for all the pulse durations. In the images three distinct zones can be identified as: 1- background or non-perturbed surrounding atmosphere; 2- shock wave with lighter shades depicting higher refractive index compared to the ambient air; 3- ablation plume, which drives the shock wave expansion. In some frames ejected material is visible and present as late as 3 µs. The images showed that the shock wave expansion was consistent throughout the observed delay range up to 5 µs; on the other hand the ablation plume expansion stopped around 1.5 µs. The size of the ablation plume was smaller

11

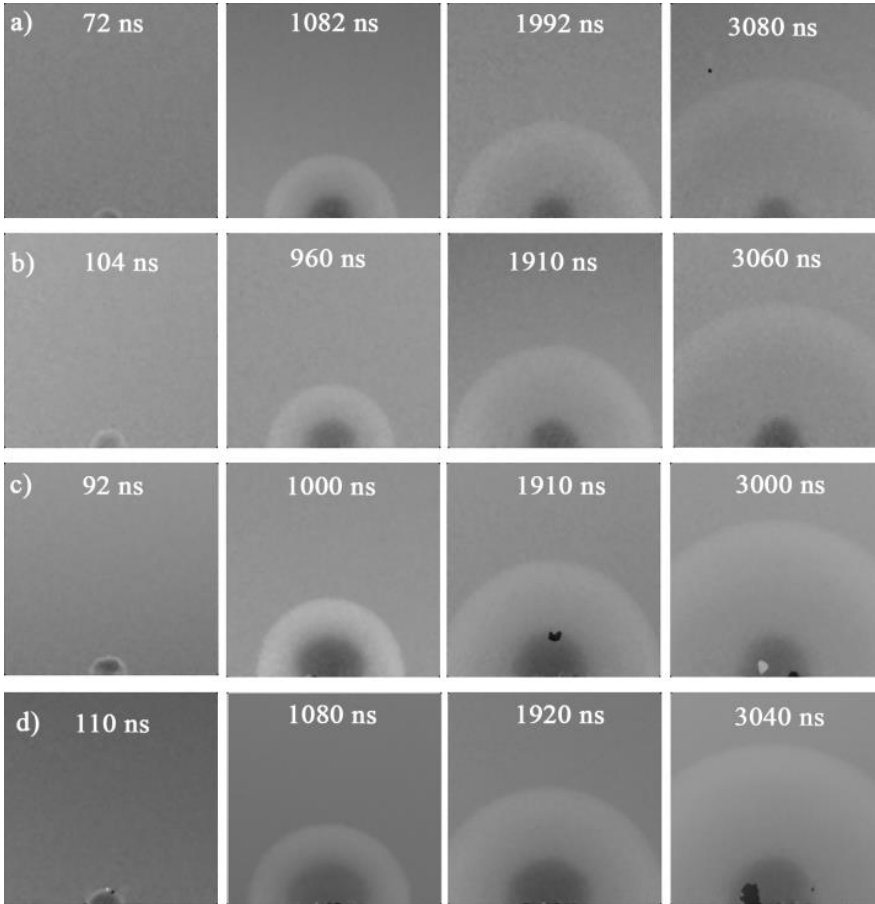for shorter pulses, implying less amount of plasma generation during ablation.

Figure 8. Shock wave expansion in intermediate delays for a) 30 ns, b) 40 ns, c) 100 ns, and d) 200 ns pulses. Field of view is 1.8 x 1.8 mm^2 in each image.

The shock wave extent differed significantly between the different pulse durations. The horizontal expansion (r_{hor}) was only recordable until approximately 2 µs after the end of the ablation pulse, due to the limited field of view. On the other hand, the vertical expansion (r_{ver}) could be recorded until approximately 5 µs within the same field of view. Shock wave expanded faster as the ablation pulse duration increased, while the horizontal and vertical extents were similar. Figure 9 shows the measured shock wave radii in horizontal and vertical extent until 2 µs. Similarity in expansion behaviour was observed for 100 and 200 ns in vertical extent, recalling the distinct groups of quality below and above 40 ns. Between 2 and 5 µs a constant expansion rate was observed, depicting the reach of terminal velocity due to the reach of equilibrium against the ambient pressure (see Figure 10). Linear regression lines were fit to predict the constant expansion rate, which was found to be in the range of 306-334 m/s (Mach I). An analogous terminal velocity was observed by Zhou *et al*

during ablation of Si with a similar fibre laser [19]. The initial speed of the shock wave measured at the first time instance was around 2 km/s (around Mach V).
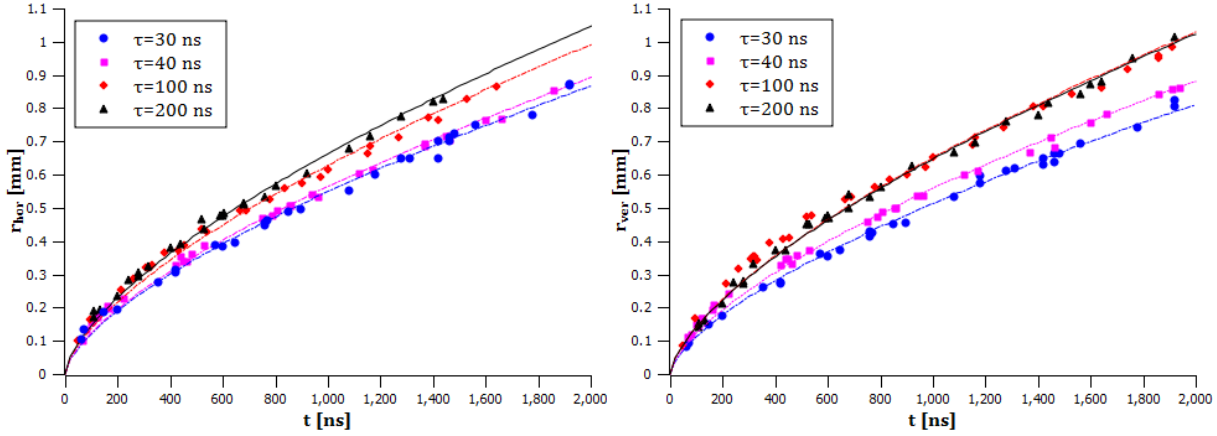

Figure 9. Shock wave radii in horizontal (r_{hor}) and vertical (r_{ver}) expansion extent for the different pulse durations as a function of time delay after the end of the pulse. The fit curves represent planar shock wave propagation ($\zeta=1$) according to blast-wave theory.
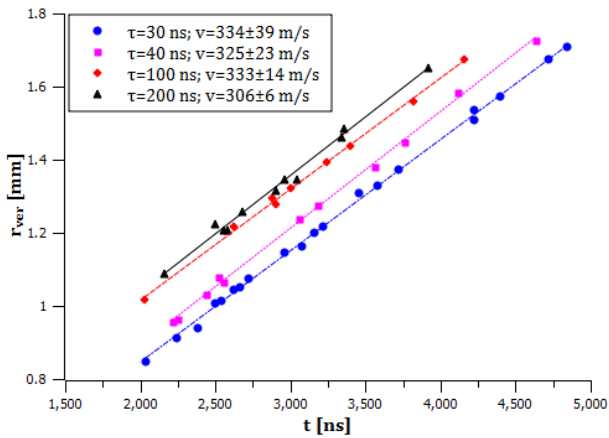

Figure 10. Shock wave radii in vertical (r_{ver}) expansion extent for the different pulse durations as a function of time delay between 2-5 μs after the ablation pulse. The expansion velocities are expressed as mean with 95% confidence intervals.

For a better comprehension of the shock wave characteristics, the results were analysed according to the Sedov-Taylor blast-wave theory [32-34].The region before the reach of terminal velocity was used for the characterization. According to the theory, for a shock wave the distance of the perimeter (r) to the explosion as function of time (t) can be expressed as:

$$r = \kappa \left(\frac{q}{\rho_0}\right)^{1/(2+\zeta)} t^{2/(2+\zeta)}$$

Eq.(1)

13

where κ is a constant close to unity, ρ_0 is the undisturbed density of air (1.25 kg/m³), ζ is the parameter that accounts for the dimensionality of the propagation with $\zeta=3$ for spherical, $\zeta=2$ for cylindrical, and $\zeta=1$ for planar propagation. Accordingly, the term q accounts for total energy (q [J]) for spherical, energy per unit length for cylindrical (q [J/cm]), and energy per unit area (q [J/cm²]) for planar propagation. The formulation can be used to estimate the symmetry in shock wave propagation, but implies that the shock wave attenuation is determined by the charge shape, *i.e.* the heat source. The data were first fit with a non-linear regression approach using statistical software (Minitab 16) with the following form:

$$r = Ct^x$$
<div align="right">Eq.(2)</div>

where the exponent $x=2/(2+\zeta)$ can be used to calculate the estimated propagation parameter, $\hat{\zeta}$. The fitting method uses an iterative algorithm (Gauss-Newton) to match the unknowns of the non-linear regression equation starting from set values, which diverges to the best fit. Along with the expected values of the unknowns, statistical confidence intervals are calculated. In Table II the x coefficients and $\hat{\zeta}$ estimated propagation parameters for the different ablation pulse durations and expansion directions are reported. It can be observed that the expansions possess mostly planar component with the shortest pulse duration (30 ns) fitting perfectly with a planar expansion behaviour. The pulse durations between 40-200 ns seem to possess also cylindrical expansion components. Although the observed shock wave shape was semi-spherical, the calculations showed the expansion behaviour was closer to planar symmetry. Yavas *et al* reported planar expansion during the ablation of calcium carbonate [35]. The authors showed that the material removal across the irradiated area was more homogenous in the presence of planar shock wave formation, and higher machining quality was obtained compared to spherical shock wave formation.

On the other hand the results can be interpreted to determine the shape of the heat source causing the shock wave. For a spherical propagation a point source would be required, whereas the planar expansion should be generated by a planar source. The use of ns pulses on TiN yield limited heat penetration depth expressed as:

$$d = \sqrt{4\tau\alpha}$$
<div align="right">Eq.(3)</div>

Table II. The estimated x coefficients and $\hat{\zeta}$ parameters of vertical and horizontal expansions of the ablation plume for the different pulse durations. Calculated ranges represent 95% confidence interval for the mean.

τ	$x=2/(2+\zeta)$		$\hat{\zeta}$	
	Vertical expansion	Horizontal expansion	Vertical expansion	Horizontal expansion
30 ns	0.66±0.03	0.69±0.02	1.03±0.13	0.82±0.08
40 ns	0.60±0.02	0.61±0.02	1.23±0.11	1.28±0.10
100 ns	0.60±0.02	0.58±0.02	1.23±0.11	1.33±0.11
200 ns	0.61±0.02	0.64±0.02	1.17±0.10	1.03±0.09

where α is the thermal diffusivity of the material (for TiN $\alpha=5.24\cdot10^{-6}$ m^2/s). Heat penetration depth can be compared to the lateral extent of the heat source, hence laser beam diameter. The laser beam diameter (d_0) can be calculated from the following equation:

$$d_0 = \frac{4}{\pi}\frac{M^2\lambda f}{d_c}$$

Eq.(4)

where M^2 is the beam quality factor, f is the focal length and d_c is the collimated beam diameter. The calculated laser beam diameter of was 25.6 μm. Table III shows the calculated heat penetration depths for the different pulse durations and the ratio of heat source (laser beam) diameter to heat penetration. The calculations show that the heat source diameter on the material plane is an order of magnitude larger than the heat penetration (up to 32 times). Being sufficiently thin with respect to the radial extent, the heat source can be approximated as planar. Thus, for further analysis planar expansion was used to estimate the q expressed in Eq.(1), which becomes energy deposited per area for $\zeta=1$. Accordingly the fit non-linear regression in Eq.(2) was modified with x=2/3. In Figure 9 the fit model for horizontal and vertical expansion extent are also shown. Using the coefficients of the fit model q was calculated from:

$$q = C^3\rho_0$$

Eq.(4)

Table III. Heat penetration depth in the TiN coating for different pulse durations, and the resultant ratio of heat source diameter ($d_0=25.6$ μm) to heat penetration depth (d).

t[ns]	d [μm]	d_0/d
30	0.79	32.4
40	0.92	27.8
100	1.45	17.6
200	2.05	12.5

The amount of energy deposited per area can be better compared with the laser fluence rather than the pulse duration. Figure 11 shows the calculated values of q as a function of average laser fluence ($F=4E/\pi d_0^2$) for both vertical and horizontal expansion extents. An exponential increase in q is observed as the laser fluence increases. The calculations showed an energy deposition between 0.02 and 0.04 J/cm^2 that acts as the energy source for the shock wave expansion. Previous works also considered a complete transformation of the laser energy to the shock wave generation and estimated the absorbed energy by the shock wave. These works report spherical expanding shock waves when high energy pulses in mJ range with ns-level durations are used. Callies *et al.* estimated the fraction of pulse energy deposited in the shockwave assuming a point explosion on metallic targets and pulse energies varying between 1.4-12 mJ and 60 ns pulses [20]. Amer et al. compared the energy component in a spherical expansion to the laser energy to estimate the energy conversion efficiency, using 15 mJ and 12 ns pulses on polycrystalline boron nitride (PCBN) [24]. Both of the works showed up to 80% conversion efficiency. Jeong *et al.* on the other hand used the same approach for calculating the energy release during the ablation of aluminium with 7 mJ and 30 ns pulses [12]. In contrast, their calculations showed overestimated energy conversion (up to 170%) for ablation under 300 Torr pressure. As a matter of fact, when high energy pulses are used, air breakdown can accompany the ablation process. These ablation conditions are likely to induce large plasma generation and hence different shock wave expansion behaviour. It can be deduced that the planar expansion behaviour is a result of lower intensity of the experimented conditions, hence less amount of energy being deposited to plasma generation. The laser beam acts as a planar heat source,

generating plasma only in the initial stage of the shock wave expansion. The plasma that transfers energy to the propagating shock wave, follows the heat source geometry of the impinging beam, therefore planar shock wave expansion is observed. Hence, the use of high brilliance fibre laser with fast ascending pulse profile can limit plasma related drawbacks such as plasma shielding, defocusing or etching. Technologically, this corresponds to higher machining quality.
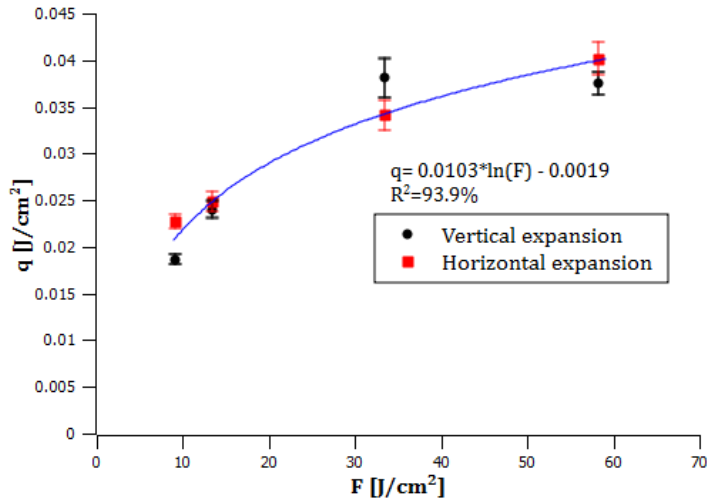

Figure 11. Energy deposited per area (q) as a function of the average laser fluence.

4. Recommendations for pulse shape design

In the light of the experimental analysis, some key recommendations can be deduced regarding the pulse design for high quality machining of TiN coating. The main concern is to avoid excessive melt and plasma generation. The reflected pulse analysis depicted some of the critical points. The first time critical time instance is regarding the pulse rise time and it is required to be shorter than 14 ns. The pulse duration for melt free ablation were determined for 30 and 40 ns durations for single pulse interactions. Between 30 and 40 ns the traces melt generation due to oscillations in the reflected pulse signal were observed. For more complex multiple pulse interactions, the accumulation of heat can be expected, hence resulting in reduced machining quality. As demonstrated previously, on the same material the pulses similar to the present 30 ns, where τ=12 ns (FWHM) exhibited melt free ablation with multiple pulses [8]. Moreover, damage accumulation behaviour, a phenomenon that reduces the ablation threshold as a function of pulse number commonly with ultrashort pulses [36] was observed. The 100 and 200 ns pulses show oscillating behaviour in the decaying tail starting from the

17

absorption peak at 14 ns and continuing until the pulse end. Actually, the oscillation is present also between 30 and 40 ns of the longer pulses due to high power levels present. This shows that not only the pulse duration but also the decaying behaviour is critical. A first possible pulse shape can be recommended for longer pulses. If increased material removal is desired, a fast ascending and descending peak of 30-40 ns duration should be accompanied by a low power level tail. This is in accordance to the observations of Pangovski et al, where such pulse shapes were more efficient in ablation of Si [7].

The shockwave expansion analysis illustrates the effect of pulse duration also in spatial domain. The presence of disc source is linked to the heat penetration depth. For higher quality machining conditions obtained with 30 and 40 ns pulses, heat penetration depth is below a quarter of the coating thickness for. Moreover, at these conditions the diameter to depth ratio of the heat source remains above 25. Hence, the machining is limited a superficial interaction removing small layers of material. If the critical ratio of the disc source is taken the empirically observed level of 25, the maximum pulse duration allowed can be calculated rewriting Eq.(3) as 50 ns, where the heat penetration depth is around 1 μm. Thus, a second pulse shape design can be recommended involving the increase of the pulse duration up to 50 ns for increased material removal. The pulse shape should be skewed towards the ascending side to respect the rise time limit.

5. Conclusions

This work aimed to provide better comprehension on ns laser pulsed machining, linking the pulse shape to temporal and spatial components of the ablation phenomenon by the use online monitoring methods. The reflected pulse analysis showed peak absorption regions for 30-200 ns pulses. Such absorption is expected to be induced by plasma absorption or melt generation, both of which are degrading factors on the micromachining quality. The analysis showed that the appearance of the absorption peak was strictly correlated to the pulse rise time that is required to be concluded below 14 ns. A fast decaying peak accompanied by a low tail was recommended if longer pulses in 100 and 200 ns range should be used to increase material removal. Digital holography images were taken for time delays up to 5 μs after the pulse initiation. The images showed smaller amount of plasma for shorter pulses, hence smaller amount of ablation plume identified by lower refractive index. Planar expansion behaviour was observed on the measured expansion radii according to the Sedov-Taylor blast-wave theory. Accordingly the deposited energy per area for shock wave expansion was

estimated around 0.02-0.04 J/cm^2, which corresponds to a very small fraction of the laser fluence. The shockwave expansion behaviour contributed to link the pulse shape characteristics to the spatial components of the ablation phenomenon. The disc source is found to be a consequence of the low intensity used in the pulses along with the ratio of laser diameter to heat penetration. An empirical critical level ($d_0/d=25$) was found to establish a limit pulse duration at 50 ns to achieve a disc source for cleaner ablation.

Large experimental analysis on the available laser micromachining parameters can improve the quality to a certain extent. Since, commonly the pulse shape is a laser source characteristic rather than a programmable feature, the end user is often limited in the quality achievable by the used laser source. The methods used in this work exhibit a straight forward approach that can be employed to design industrial laser systems that are tuned to the material interaction. In the exhibited case study on TiN, two pulse shapes were recommended for further improving the machining productivity without compromising the quality. The approach can be extended to other materials. With the further spread of newer pulse shape programmable lasers, new temporal pulse shapes for advanced applications can be integrated in a plug and play manner.

References

1.   R. E. Russo, X. Mao, H. Liu, J. Gonzalez, and S. S. Mao, "Laser ablation in analytical chemistry-a review", *Talanta*, vol. 57, pp. 425–451, 2002.

2.   G.W. Yang, "Laser ablation in liquids: Applications in the synthesis of nanocrystals", *Prog. Mater. Sci.*, vol.52, pp. 648–69, 2007.

3.   M. N. R. Ashfold, F. Claeyssens, G. M. Fuge, and Simon J. Henley, "Pulsed laser ablation and deposition of thin films", *Chem. Soc. Rev.,* vol. 33 , pp. 23 – 31, 2004.

4.   R. Eason, "Pulsed Laser Deposition of Thin Films: Applications-Led Growth of Functional Materials", John Wiley & Sons, Hoboken, NJ, 2007

5.   A. Vogel and V. Venugopalan, "Mechanisms of pulsed laser ablation of biological tissues", *Chem. Rev.,* vol. 103, pp. 577-644, 2003.

6.   H. J. Booth, "Recent applications of pulsed lasers in advanced materials processing", *Thin Solid Films*, vol. 453 –454, pp. 450–457, 2004.

7.   K. Pangovski, M. Sparkes, A. Cockburn, W. O'Neill, P. S. The, D. Lin, and D. Richardson, "Control of Material Transport Through Pulse Shape Manipulation - A Development Toward Designer Pulses", *IEEE J. Sel. Topics Quantum Electron.,* vol. 20, no. 5, 2014.

8.   A.G. Demir, K. Pagovski, B. Previtali, W. O'Neill, "Laser micromachining of TiN coatings with variable pulse durations and shapes in ns regime", *Surf. Coat. Tech.*, vol. 258, 240–248, 2014

9.   B. N. Chichkov, C. Momma, S. Nolte, F. Von Alvensleben, and A. Tünnermann, "Femtosecond, picosecond and nanosecond laser ablation of solids", *Appl. Phys. A*, vol. 63, no. 2 pp. 109-115, 1996.

10. N. Bityurin, B. S. Luk'yanchuk, M. H. Hong, and T. C. Chong, "Models for Laser Ablation of Polymers", *Chem. Rev.*, vol. 103, pp. 519-552, 2003.

11. L. V. Zhigilei, E. Leveugle, B. J. Garrison, Y. G. Yingling, and M. I. Zeifman, "Computer Simulations of Laser Ablation of Molecular Substrates", *Chem. Rev.*, vol. 103, pp. 321-347, 2003.

12. S. H. Jeong, R. Greif, and R. E. Russo, "Shock wave and material vapour plume propagation during excimer laser ablation of aluminium samples", *J. Phys. D. Appl. Phys.*, vol. 32, no. 19, pp. 2578–2585, 1999.

13. R. Petkovšek and P. Gregorčič, "A laser probe measurement of cavitation bubble dynamics improved by shock wave detection and compared to shadow photography", *J. Appl. Phys.*, vol. 102, no. 4, p. 044909, 2007.

14. J. H. Yoo, S. H. Jeong, R. Greif, and R. E. Russo, "Explosive change in crater properties during high power nanosecond laser ablation of silicon," *J. Appl. Phys.*, vol. 88, no. 3, p. 1638, 2000.

15. X. Zeng, X. L. Mao, R. Greif, and R. E. Russo, "Experimental investigation of ablation efficiency and plasma expansion during femtosecond and nanosecond laser ablation of silicon," *Appl. Phys. A*, vol. 80, no. 2, pp. 237–241, 2004.

16. D. J. Hwang, C. P. Grigoropoulos, and T. Y. Choi, "Efficiency of silicon micromachining by femtosecond laser pulses in ambient air", *J. Appl. Phys.*, vol. 99, no. 8, p. 083101, 2006.

17. T. Tsuji, Y. Okazaki, Y. Tsuboi, and M. Tsuji, "Nanosecond Time-Resolved Observations of Laser Ablation of Silver in Water", *Jpn. J. Appl. Phys.*, vol. 46, no. 4A, pp. 1533–1535, 2007.

18. J.-F. Y. Gravel and D. Boudreau, "Study by focused shadowgraphy of the effect of laser irradiance on laser-induced plasma formation and ablation rate in various gases", *Spectrochim. Acta Part B At. Spectrosc.*, vol. 64, no. 1, pp. 56–66, 2009.

19. Y. Zhou, B. Wu, S. Tao, A. Forsman, and Y. Gao, "Physical mechanism of silicon ablation with long nanosecond laser pulses at 1064nm through time-resolved observation", *Appl. Surf. Sci.*, vol. 257, no. 7, pp. 2886–2890, 2011.

20. G. Callies, P. Berger, H. Huegel, "Time-resolved observation of gas-dynamic discontinuities arising during excimer laser ablation and their interpretation", *J. Phys. D: Appl. Phys.,* vol. 28 pp.794-806, 1995.

21. H. Schittenhelm, G. Callies, P. Berger, and H. Hugel, "Two-wavelength interferometry on excimer laser induced vapour r plasma plumes during the laser pulse", *Appl. Surf. Sci.* vol. 127-129, pp. 922–927, 1998.

22. R. E. Russo, X. L. Mao, H. C. Liu, J. H. Yoo, and S. S. Mao, "Time-resolved plasma diagnostics and mass removal during single-pulse laser ablation," *Appl. Phys. A,* vol. 69, [Suppl.] pp. S887–S894, 1999.

23. P. Gren, "Four-pulse interferometric recordings of transient events by pulsed TV holography", *Opt. Lasers Eng.*, vol. 40, no. 5–6, pp. 517–528, 2003.

24. E. Amer, P. Gren, and M. Sjödahl, "Shock wave generation in laser ablation studied using pulsed digital holographic interferometry", *J. Phys. D. Appl. Phys.*, vol. 41, no. 21, 215502 (9 pp), 2008.

25. E. Amer, P. Gren, and M. Sjödahl, "Laser-ablation-induced refractive index fields studied using pulsed digital holographic interferometry", *Opt. Lasers Eng.*, vol. 47, no. 7–8, pp. 793–799, 2009.

26. E. Amer, P. Gren, a. F. H. Kaplan, M. Sjödahl, and M. El Shaer, "Comparison of the laser ablation process on Zn and Ti using pulsed digital holographic interferometry", *Appl. Surf. Sci.*, vol. 256, no. 14, pp. 4633–4641, 2010.

27. S. Hogmark, S. Jacobson, M. Larsson, "Design and evaluation of tribological coatings", *Wear,* vol. 1-2, pp.20–33, 2000.

28. A.J. Dowling, M.K. Ghantasala, J.P. Hayes, E.C. Harvey, E.D. Doyle, "Excimer laser micromachining of TiN films from chromium and copper sacrificial layers", *Smart Mater. Struct.,* vol. 11, pp.715–721, 2002.

29. H.C. Man, Q.Wang, X.Guo, "Laser surface microdrilling of Ti and laser gas nitride Ti for enhancing fixation of dental implants", *Opt. Lasers Eng.,,* vol.48, pp.583–588, 2010.

30. B. Xu, Q. Wang, X. Zhang, S. Zhao, Y. Xia, L. Mei, X. Wang, and G. Wang, "Impulse transfer to the surface of aluminum and copper from a pulsed Nd: YAG laser", *Appl. Phys. B Photophysics Laser Chem.*, vol. 57, no. 4, pp. 277–280, 1993.

31. R.G. Root, "Modeling of Post-Breakdown in Laser-Induced Plasmas and Applications, in Laser induced plasmas and applications", Eds L.Z. Radziemski, D.A. Cremers, Dekker, New York, 1989

32. G. Taylor, "The formation of a blast wave by a very intense explosion I . Theoretical discussion", *Proc. R. Soc. A Math. Phys. Eng. Sci.*, vol. 201, no. 1065, pp. 159–174, 1950.

33. G. Taylor, "The Formation of a Blast Wave by a Very Intense Explosion. II. The Atomic Explosion of 1945", *Proc. R. Soc. A Math. Phys. Eng. Sci.*, vol. 201, no. 1065, pp. 175–186, 1950.

34. L. I. Sedov, Similarity and Dimensional Methods in Mechanics, 10th Ed, 1993, CRC Press Florida

35. O. Yavas, E. L. Maddocks, M. R. Papantonakis, and R. F. Hanglund, "Planar and spherical shock wave generation during infrared laser ablation of calcium carbonate", *Appl. Surf. Sci.* vol. 127–129, pp. 26–32, 1998.

36. P.T. Mannion, J. Magee, E. Coyne, G.M. O'Connor, and T.J. Glynn. "The effect of damage accumulation behaviour on ablation thresholds and damage morphology in ultrafast laser micro-machining of common metals in air", *Appl. Surf. Sci.* vol. 233, pp.275–287, 2004.